WALAILAK JOURNAL
http://wjst.wu.ac.th Engineering and Physical Sciences

Discretization Techniques of Height Function Method for Greater Increased Accuracy of Mass Conservation

Boonchai LERTNUWAT

Department of Mechanical Engineering, Chulalongkorn University, Bangkok 10330, Thailand

(Corresponding author; e-mail: boonchai.l@chula.ac.th)

Received: 25 April 2013, Revised: 22 January 2014, Accepted: 10 March 2014

Abstract

A height function method has been used to solve the shape of free surfaces in incompressible viscous flows for hydrodynamics. Three proposed discretization techniques for the height function method are developed with particular attention to the law of mass conservation. The concept of the proposed techniques is to place a control volume on the most appropriate location in any staggered grid system. First, the proposed techniques and the conventional technique are verified with a simple problem whose exact solution is known. Then, all numerical techniques are examined with a more complicated problem to investigate their accuracy. The simulated results of the proposed techniques are compared to those of conventional technique. Finally, it is concluded that (1) the proposed techniques will give better results than the conventional technique if the grid resolution is sufficiently fine, (2) the first proposed technique gives poorer results than the other proposed techniques, and (3) the second proposed technique gives better results than the third proposed technique, but the third proposed technique is easier to apply due to its explicit form of the equation.

Keywords: Finite volume method, free surface, height function method, hydrodynamic, two-phase flow

Nomenclature

Alphabets

A	Area
B	Bottom
b	Flow depth
C	Chord
c	Grid velocity
CV	Control volume
f	Body force per unit mass
g	Gravity acceleration
H	Height function
L	Length
$\dot{m}$	Mass flux
p	Static pressure
$\tilde{p}$	Hydrodynamic pressure
R	Radius
t	Time
u	Velocity component on x-direction
V	Velocity
w	Velocity component on z-direction
x	Location on x-direction
z	Location on z-direction
δ	Film thickness
μ	Liquid viscosity
θ	Incline's angle
ρ	Liquid density
σ	Surface tension

Superscripts and Subscripts

c	Center of grid cell
F	Free surface
i	Horizontal spatial index
k	Vertical spatial index
l	Liquid
n	(superscript) Time index
n	(subscript) Normal
t	Tangent
v	Vertex of gridlines
W	Wall

Introduction

Flows in nature sometimes occur not only with one fluid but also with several fluids interacting in a flow. When the 2 fluids are a gas and a liquid the interface between these 2 fluids could be considered as a free surface since the viscosity of gases is much less than the viscosity of liquids [1,2]. Flows in which any free surface exists are called free surface flows which have long been studied with experimental and numerical methods [3-9].

Numerical methods can be briefly divided into 2 groups, namely interface-tracking methods and interface-capturing methods [10]. Interface-tracking methods solve problems of free surface flows by following the movement of free surface directly. The height function method [11] and surface marker method [12,13] are categorized as interface-tracking methods. In a different way, interface-capturing methods solve problems of free surface flows by calculating other parameters which are eventually used to predict the shape of free surfaces. Examples of these parameters include markers in the marker-and-cell (MAC) method [14,15] and fluid volume fraction in the volume-of-fluid (VOF) method [16,17].

It is well-known that interface-tracking methods cannot predict the complicated shapes of free surfaces, unlike interface-capturing methods. However, interface-tracking methods are sometimes suitable for use with problems where free surfaces are not complicated but where the tension effect is important. Nevertheless, many researchers have recently tried to develop techniques using interface-capturing methods (VOF method) with interface-tracking methods (height function method) as a supplement, but the tension effect is still taken into account separately [18-22].

The height function method, which is a familiar interface-tracking method, is used in the current research work in order to give better results on mass conservation. Details of the developed techniques and the verification of the developed techniques are successively presented. Finally, all developed techniques are examined to investigate their accuracy.

Mathematical formulation

There are basically 2 types of governing equation for calculating height function, i.e. the kinematic boundary condition and the conservative form of the free surface equation. The latter one is usually selected when mass conservation needs to be rigorously maintained which is the objective of this work. The conservative form of the free surface equation is thus employed to investigate how it can be improved. Although the original equation is 3 dimensional, for the sake of simplicity, when its results are analyzed, it is reduced to be 2 dimensional, i.e.;

$$\frac{\partial H}{\partial t}+\frac{\partial}{\partial x}\int_{B}^{H} u dz = 0 \,. \tag{1}$$

The velocity in the z-direction (w) will be not taken into account because it does not affect flow rate if controlled volumes are drawn with 2 vertical lines on the left and right hand side as shown in **Figure 2**. This is because flow rate $= \int_{B}^{H}\left\{\vec{V}\cdot d\vec{A}\right\} = \int_{B}^{H}\left\{\left[u\hat{i}+w\hat{k}\right]\cdot\left[\left(dz\right)\hat{i}+\left(0\right)\hat{k}\right]\right\} = \int_{B}^{H} u dz$.

Staggered grids (as shown in **Figure 1**) are often exploited for solving problems of free surface flows. When Eq. (1) is numerically used, it must be discretized to be compatible with an exploited grid system. It is conventionally discretized as;

$$H_{i_v}^{n+1} = H_{i_v}^{n} - \frac{\Delta t}{\Delta x_{i_v}}\left[\sum_{k=1}^{k_{\max}}\left(u_{i_v,k}^{+}\Delta z_{i_v,k}^{+} - u_{i_v,k}^{-}\Delta z_{i_v,k}^{-}\right)\right] \tag{2}$$

where

$$\Delta x_{i_v} = \left(x^n_{v,i_v+1,0} - x^n_{v,i_v-1,0}\right)\Big/2,$$
$$\Delta z^-_{i_v,k_v} = \left(z^n_{v,i_v-1,k_v} + z^n_{v,i_v,k_v} - z^n_{v,i_v-1,k_v-1} - z^n_{v,i_v,k_v-1}\right)\Big/2,$$
$$\Delta z^+_{i_v,k_v} = \left(z^n_{v,i_v,k_v} + z^n_{v,i_v+1,k_v} - z^n_{v,i_v,k_v-1} - z^n_{v,i_v+1,k_v-1}\right)\Big/2,$$
$$u^-_{i_v,k_c} = \left(u^n_{i_v-1,k_c} + u^n_{i_v,k_c}\right)\Big/2,$$
$$u^+_{i_v,k_c} = \left(u^n_{i_v,k_c} + u^n_{i_v+1,k_c}\right)\Big/2,$$

in accordance with the control volume shown in **Figure 2a**. In this case the velocities on cell faces ($u^-_{i_v,k_c}$ and $u^+_{i_v,k_c}$) can be determined by averaging from 2 nodes of horizontal velocity on their left and right hand sides because all Δx's in each grid are equal. If Δx's are not equal, interpolation will be needed.

If we know the average variables, i.e. Δx_{i_v}, $\Delta z^-_{i_v,k}$, $\Delta z^+_{i_v,k}$, $u^-_{i_v,k}$ and $u^+_{i_v,k}$, Eq. (2) will explicitly give us the height function at position i_v in the next time step without considering the adjacent height function. This is because the conventional method assumes that $H^{n+1}_{i_v-1}$, $H^{n+1}_{i_v}$ and $H^{n+1}_{i_v+1}$ change their value with the same height difference. This is not correct because each height function does not need to change with the same height difference. Although some research, e.g. [11], has exploited techniques of spline curves to smooth free surface curves, the techniques do not consider the law of mass conservation. New discretization techniques are, thus, developed to conserve mass in the system of free surface flow. The first proposed technique is developed by considering the different changes of the adjacent height functions. According to **Figure 2a**, the control volume is generally pentagonal, the change of the control volume should be written as;

$$\frac{1}{4\Delta t}\left[\left(H^{n+1}_{i_v-1}+3H^{n+1}_{i_v}\right)\Delta x^-_{i_v} + \left(3H^{n+1}_{i_v}+H^{n+1}_{i_v+1}\right)\Delta x^+_{i_v} - \left(H^{n}_{i_v-1}+3H^{n}_{i_v}\right)\Delta x^-_{i_v} - \left(3H^{n}_{i_v}+H^{n}_{i_v+1}\right)\Delta x^+_{i_v}\right]$$
$$+\left[\sum_{k=1}^{k_{\max}}\left(u^+_{i_v,k}\Delta z^+_{i_v,k} - u^-_{i_v,k}\Delta z^-_{i_v,k}\right)\right] = 0 \qquad (3)$$

or

$$A_{i_v}H^{n+1}_{i_v-1} + B_{i_v}H^{n+1}_{i_v} + C_{i_v}H^{n+1}_{i_v+1} = A_{i_v}H^{n}_{i_v-1} + B_{i_v}H^{n}_{i_v} + C_{i_v}H^{n}_{i_v+1} - \Theta_{i_v} \qquad (4)$$

where

$$A_{i_v} = \Delta x^-_{i_v},$$
$$B_{i_v} = 3\left(\Delta x^-_{i_v} + \Delta x^+_{i_v}\right),$$
$$C_{i_v} = \Delta x^+_{i_v},$$
$$\Theta_{i_v} = 4\Delta t\sum_{k=1}^{k_{\max}}\left(u^+_{i_v,k}\Delta z^+_{i_v,k} - u^-_{i_v,k}\Delta z^-_{i_v,k}\right),$$
$$\Delta x^-_{i_v} = \left(x^n_{v,i_v,0} - x^n_{v,i_v-1,0}\right)\Big/2,$$

$$\Delta x_{i_v}^{+} = \left(x_{v,i_v+1,0}^{n} - x_{v,i_v,0}^{n} \right) \Big/ 2 ,$$
$$\Delta z_{i_v,k_v}^{-} = \left(z_{v,i_v-1,k_v}^{n} + z_{v,i_v,k_v}^{n} - z_{v,i_v-1,k_v-1}^{n} - z_{v,i_v,k_v-1}^{n} \right) \Big/ 2 ,$$
$$\Delta z_{i_v,k_v}^{+} = \left(z_{v,i_v,k_v}^{n} + z_{v,i_v+1,k_v}^{n} - z_{v,i_v,k_v-1}^{n} - z_{v,i_v+1,k_v-1}^{n} \right) \Big/ 2 ,$$
$$u_{i_v,k_c}^{-} = \left(u_{i_v-1,k_c}^{n} + u_{i_v,k_c}^{n} \right) \Big/ 2 ,$$
$$u_{i_v,k_c}^{+} = \left(u_{i_v,k_c}^{n} + u_{i_v+1,k_c}^{n} \right) \Big/ 2 .$$

So far, the first technique shown in Eq. (4) takes into account the adjacent height functions and is likely to give better results. Nevertheless, it still uses interpolated variables (i.e. Δx_{i_v}, $\Delta z_{i_v,k}^{-}$, $\Delta z_{i_v,k}^{+}$, $u_{i_v,k}^{-}$ and $u_{i_v,k}^{+}$) which may cause some errors. The second proposed technique is developed to prevent error by drawing each control volume so that it is coincident with the gridlines as shown in **Figure 2b**. The governing equation of height function which is compatible with the control volume can be written as;

$$\frac{1}{2\Delta t}\left[\left(H_{i_v-1}^{n+1} + H_{i_v}^{n+1} \right) \Delta x_{i_v}^{-} + \left(H_{i_v}^{n+1} + H_{i_v+1}^{n+1} \right) \Delta x_{i_v}^{+} - \left(H_{i_v-1}^{n} + H_{i_v}^{n} \right) \Delta x_{i_v}^{-} - \left(H_{i_v}^{n} + H_{i_v+1}^{n} \right) \Delta x_{i_v}^{+} \right]$$
$$+ \left[\sum_{k=1}^{k_{\max}} \left(u_{i_v,k}^{+} \Delta z_{i_v,k}^{+} - u_{i_v,k}^{-} \Delta z_{i_v,k}^{-} \right) \right] = 0 \qquad (5)$$

or

$$A_{i_v} H_{i_v-1}^{n+1} + B_{i_v} H_{i_v}^{n+1} + C_{i_v} H_{i_v+1}^{n+1} = A_{i_v} H_{i_v-1}^{n} + B_{i_v} H_{i_v}^{n} + C_{i_v} H_{i_v+1}^{n} - \Theta_{i_v} \qquad (6)$$

where

$$A_{i_v} = \Delta x_{i_v}^{-} ,$$
$$B_{i_v} = \Delta x_{i_v}^{-} + \Delta x_{i_v}^{+} ,$$
$$C_{i_v} = \Delta x_{i_v}^{+} ,$$
$$\Theta_{i_v} = 2\Delta t \sum_{k=1}^{k_{\max}} \left(u_{i_v,k}^{+} \Delta z_{i_v,k}^{+} - u_{i_v,k}^{-} \Delta z_{i_v,k}^{-} \right) ,$$
$$\Delta x_{i_v}^{-} = x_{v,i_v,0}^{n} - x_{v,i_v-1,0}^{n} ,$$
$$\Delta x_{i_v}^{+} = x_{v,i_v+1,0}^{n} - x_{v,i_v,0}^{n} ,$$
$$\Delta z_{i_v,k_v}^{-} = z_{v,i_v-1,k_v}^{n} - z_{v,i_v-1,k_v-1}^{n} ,$$
$$\Delta z_{i_v,k_v}^{+} = z_{v,i_v+1,k_v}^{n} - z_{v,i_v+1,k_v-1}^{n} ,$$
$$u_{i_v,k_c}^{-} = u_{i_v-1,k_c}^{n} ,$$
$$u_{i_v,k_c}^{+} = u_{i_v+1,k_c}^{n} .$$

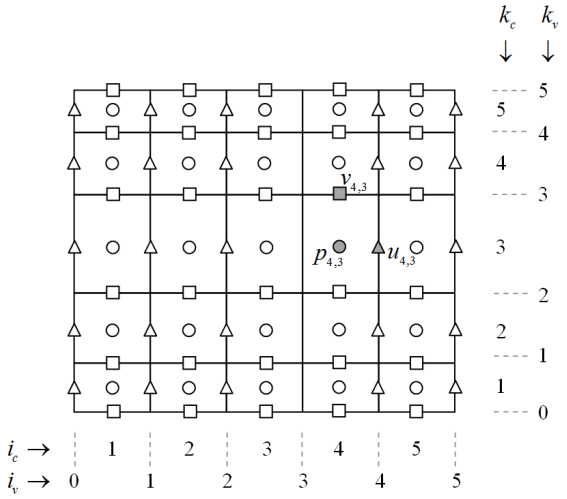

Figure 1 Example of the staggered grid system used in this work; circles, triangles and squares indicate the positions of pressure, horizontal velocity and vertical velocity, respectively.

Both Eqs. (4) and (6) are simultaneous equations which require some effort and resource to be solved. The third proposed technique is developed to avoid this problem by drawing each control volume so that it is coincident with successive vertical gridlines as shown in **Figure 2c**.

$$\frac{1}{2\Delta t}\left[\left(H_{i_v-1}^{n+1}+H_{i_v}^{n+1}\right)\Delta x_{i_v}-\left(H_{i_v-1}^{n}+H_{i_v}^{n}\right)\Delta x_{i_v}\right]+\left[\sum_{k=1}^{k_{\max}}\left(u_{i_v,k}^{+}\Delta z_{i_v,k}^{+}-u_{i_v,k}^{-}\Delta z_{i_v,k}^{-}\right)\right]=0 \tag{7}$$

or

$$\Delta x_{i_v} H_{i_v-1}^{n+1}+\Delta x_{i_v} H_{i_v}^{n+1}=\Delta x_{i_v} H_{i_v-1}^{n}+\Delta x_{i_v} H_{i_v}^{n}-\Theta_{i_v} \tag{8}$$

where

$$\Theta_{i_v}=2\Delta t\sum_{k=1}^{k_{\max}}\left(u_{i_v,k}^{+}\Delta z_{i_v,k}^{+}-u_{i_v,k}^{-}\Delta z_{i_v,k}^{-}\right),$$

$$\Delta x_{i_v}=x_{v,i_v,0}^{n}-x_{v,i_v-1,0}^{n},$$

$$\Delta z_{i_v,k_v}^{-}=z_{v,i_v-1,k_v}^{n}-z_{v,i_v-1,k_v-1}^{n},$$

$$\Delta z_{i_v,k_v}^{+}=z_{v,i_v,k_v}^{n}-z_{v,i_v,k_v-1}^{n},$$

$$u_{i_v,k_c}^{-}=u_{i_v-1,k_c}^{n},$$

$$u_{i_v,k_c}^{+}=u_{i_v,k_c}^{n}.$$

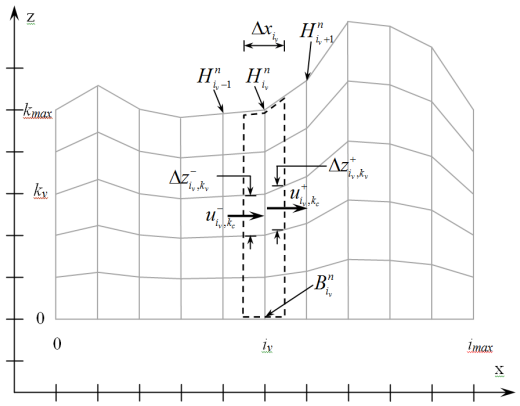

(a) Controlled volume for the conventional method and the 1st proposed technique.

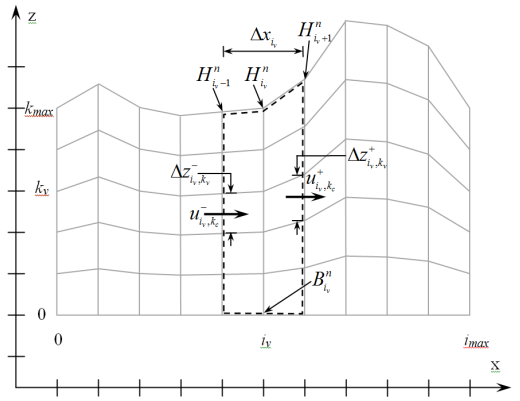

(b) Controlled volume for the 2nd proposed technique.

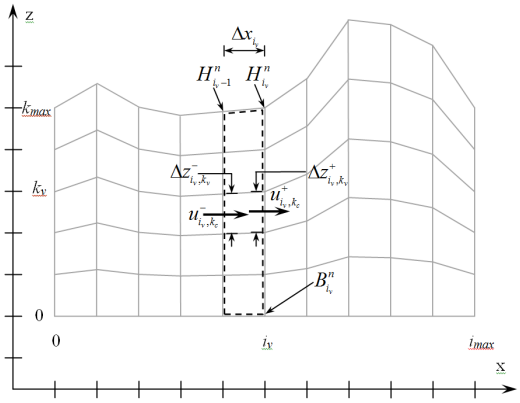

(c) Controlled volume for the 3rd proposed technique.

Figure 2 Schematic diagram showing a control volume (dash line) used for computing the height function at position i_y with the conventional method and the proposed techniques.

The value of the height function at position i_v ($H_{i_v}^{n+1}$) can be explicitly obtained from Eq. (8) if the value of the height function at position $i_v - 1$ ($H_{i_v-1}^{n+1}$) is given and vice versa. This means that all height functions can be simply determined if the value of a height function at either position $i_v = 0$ or $i_v = i_{\max}$ is given as a boundary condition.

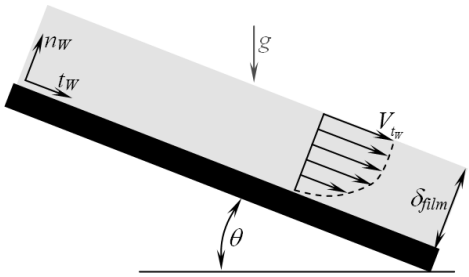

Figure 3 Schematic diagram showing a thin film flow over an incline and its dimensions used for verifying the proposed techniques.

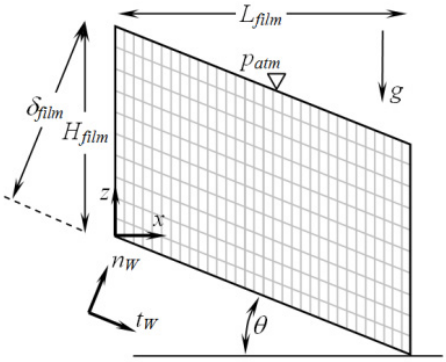

Figure 4 Computational domain of a thin film flow over an incline.

Verification with a simple problem

The proposed techniques derived in the former section are going to be verified in this section with the use of a simple problem. The problem of a thin film flow over an incline (**Figure 3**) is chosen since its exact solution is already known. The exact solution is derived from the continuity equation and Navier-Stokes equations whose reference axes are normal and tangential to the incline, i.e.;

$$\frac{\partial V_{t_W}}{\partial t_W} + \frac{\partial V_{n_W}}{\partial n_W} = 0 , \tag{9}$$

$$\rho \frac{\partial V_{t_W}}{\partial t} + \rho V_{t_W} \frac{\partial V_{t_W}}{\partial t_W} + \rho V_{n_W} \frac{\partial V_{t_W}}{\partial n_W} = -\frac{\partial p}{\partial t_W} + \mu \left[\frac{\partial^2 V_{t_W}}{\partial t_W^2} + \frac{\partial^2 V_{t_W}}{\partial n_W^2} \right] + \rho f_{t_W} , \tag{10}$$

$$\rho\frac{\partial V_{n_W}}{\partial t}+\rho V_{t_W}\frac{\partial V_{n_W}}{\partial t_W}+\rho V_{n_W}\frac{\partial V_{n_W}}{\partial n_W}=-\frac{\partial p}{\partial n_W}+\mu\left[\frac{\partial^2 V_{n_W}}{\partial t_W^2}+\frac{\partial^2 V_{n_W}}{\partial n_W^2}\right]+\rho f_{n_W}. \tag{11}$$

By assuming that (i) the flow is steady, incompressible, laminar, fully developed; (ii) the interface between the incline and the liquid is a no-slip wall and (iii) the interface between the liquid and gas is a free surface along which the pressure gradient is equal to zero, this yields the exact solution of a thin film flow over an incline, i.e.;

$$V_{t_W}=\frac{\rho g\sin\theta}{2\mu}\left(2\delta_{film}n_W-n_W^2\right), \tag{12}$$

$$V_{n_W}=0, \tag{13}$$

$$p=\rho g\left(\delta_{film}-n_W\right)\cos\theta+p_{atm}. \tag{14}$$

As a result, velocity along the x-axis (u), velocity along the y-axis (v) and hydrodynamic pressure ($\tilde{p}$) can be calculated as follows;

$$u=V_{t_W}\cos\theta+V_{n_W}\sin\theta=\frac{\rho g\sin\theta\cos\theta}{2\mu}\left(2\delta_{film}n_W-n_W^2\right), \tag{15}$$

$$w=-V_{t_W}\sin\theta+V_{n_W}\cos\theta=\frac{\rho g\sin^2\theta}{2\mu}\left(2\delta_{film}n_W-n_W^2\right), \tag{16}$$

$$\tilde{p}=p-\rho g\left(H-z\right)=\rho g\left(\delta_{film}-n_W\right)\cos\theta+p_{atm}-\rho g\left(H-z\right)=\left(\cos^2\theta-1\right)\rho g\left(H-z\right)+p_{atm}. \tag{17}$$

when the problem is numerically solved, a computational domain has to be set. **Figure 4** shows the computational domain confining a flow field whose upper, lower, left and right boundaries are a free surface, a no-slip wall, an inflow and an outflow, respectively. The grid shown in **Figure 4** is the coarsest employed resolution, namely 30×10. Gridlines evenly divide the domain in order to get rid of any advantages and disadvantages relevant to grid structure when the computational results are finally compared. Herein, the value of the variables in the figure is assigned as g = 9.81 m/s^2, p_{atm} = 0 Pa, L_{film} = 3 cm, H_{film} = 1 mm and θ = 1°. The liquid in the flow is water at 25 °C so its density and viscosity are 997.13 kg/m^3 and 0.891×10^{-3} kg/m·s. The surface tension between water and air on the free surface is assigned to be 72.14×10^{-3} N/m.

Solving the problem numerically requires a governing equation set composed of 4 equations, i.e.;

$$\oint\left(u\hat{i}+w\hat{k}\right)\cdot d\vec{L}=0, \tag{18}$$

$$\rho\left[\frac{\partial}{\partial t}\int_{CV} w dA - c_z \oint w\hat{k}\cdot d\vec{L} + \oint w\left(u\hat{i}+w\hat{k}\right)\cdot d\vec{L}\right] \tag{19}$$

$$= -\oint\left(\tilde{p}\hat{k}\right)\cdot d\vec{L} + \mu\oint\left(\frac{\partial w}{\partial x}\hat{i}+\frac{\partial w}{\partial z}\hat{k}\right)\cdot d\vec{L},$$

$$\rho\left[\frac{\partial}{\partial t}\int_{CV} u dA - c_z \oint u\hat{k}\cdot d\vec{L} + \oint u\left(u\hat{i}+w\hat{k}\right)\cdot d\vec{L}\right] \tag{20}$$

$$= -\rho g\oint\left(H\hat{i}\right)\cdot d\vec{L} - \oint\left(\tilde{p}\hat{i}\right)\cdot d\vec{L} + \mu\oint\left(\frac{\partial u}{\partial x}\hat{i}+\frac{\partial u}{\partial z}\hat{k}\right)\cdot d\vec{L}$$

$$\frac{\partial H}{\partial t} + \frac{\partial}{\partial x}\int_{B}^{H} u dz = 0, \tag{21}$$

which are continuity equation, momentum equations and the conservative form of the free surface equation, respectively. In this work, a pressure-correction method is exploited to discretize the set of equations from Eqs. (18) to (20). Meanwhile, Eq. (21) is discretized by 4 techniques, i.e. Eqs. (2), (4), (6) and (8).

Since the boundary condition on the upper side of the computational domain is a free surface, variables must be satisfied with kinetic and dynamic conditions [23], namely;

$$V_{l,n_F}\Big|_F = V_{F,n_F}, \tag{22}$$

$$\left(\frac{\partial V_{l,t_F}}{\partial n_F} + \frac{\partial V_{l,n_F}}{\partial t_F}\right)\Bigg|_F = 0, \tag{23}$$

$$p_{l,F} = p_{atm} + \sigma_F\frac{1}{R_F} + 2\mu\left(\frac{\partial V_{l,n_F}}{\partial n_F}\right)\Bigg|_F, \tag{24}$$

where $\dfrac{1}{R_F} = \left\{\dfrac{\partial^2 z}{\partial x^2}\Big|_F\left[1+\left(\dfrac{\partial z}{\partial x}\Big|_F\right)^2\right]^{-\frac{3}{2}}\right\}$.

Next, the variables on the lower side of the computational domain must be satisfied with a no slip condition, namely velocity is zero and;

$$\frac{\partial\tilde{p}}{\partial n_W}\Big|_{wall} = -\rho g\frac{\partial H}{\partial n_W}\Big|_{wall}. \tag{25}$$

Then, the velocities along the inflow boundary condition on the left side of the computational domain can be determined with Eqs. (15) and (16). In addition, the height function is consistently assigned to be

H_{film} so that the mass flux across the boundary will be constant. Whereas the pressure on this boundary must satisfy the condition;

$$\left.\frac{\partial \tilde{p}}{\partial t_W}\right|_{inflow} = 0 . \tag{26}$$

Finally the outflow boundary condition is posed on the right side of the computational domain. Subsequently, the velocity and hydrodynamic pressure must satisfy;

$$\left.\frac{\partial V}{\partial t_W}\right|_{outflow} = 0 , \tag{27}$$

$$\tilde{p}_{outflow} = \left(\cos^2\theta - 1\right)\rho g\left(H_{outflow} - z\right) + p_{l,F} . \tag{28}$$

If it is possible, height functions on the boundary will be calculated. Otherwise, linear extrapolation is employed.

The initial condition is set to be close to the exact solution. This means that velocities and hydrodynamic pressure are initially approximated with Eqs. (15), (16) and (17). The height function is set with a value so that the free surface is parallel to the incline with an offset of δ_{film}.

At first, a coarse grid (30×10 resolution) is employed. The velocity fields shown in **Figures 5a** to **5d** are computed from the 4 different numerical techniques. Looking at these 4 velocity fields, we find that they are similar: namely, all flows adjust themselves within the region close to the inflow boundary leading to oscillations of the free surfaces before they become fully developed downstream. However, it seems that the conventional technique gives the smallest oscillation of the free surface which is the closest to the exact solution. This is clearer in **Figure 6a**, which shows that the free surface curve obtained from the conventional technique is the closest to the exact solution. Although the free surface curves obtained from the proposed techniques are further from the exact solution, they still remain in relative proximity.

Considering the free surface curves in the downstream region of **Figure 6a**, we find that all curves are straight with similar steepness but different heights. This is interesting because different heights of the free surface may cause different velocity profiles as well as cross-sectional mass fluxes, which is a central concept of this work. According to **Figures 3** and **4** and Eq. (15), the exact cross-sectional mass flux per unit depth can be calculated with;

$$\frac{\dot{m}}{b} = \int_0^{H_{film}} \rho u dz = \frac{\rho^2 g \sin\theta}{3\mu}\left(H_{film}\cos\theta\right)^3 = 6.37\times10^{-2} , \tag{29}$$

and numerically estimated with;

$$\left(\frac{\dot{m}}{b}\right)_{i_v} = \sum_{k=1}^{k_{\max}} \rho u_{i_v,k}\left(z_{v,i_v,k} - z_{v,i_v,k-1}\right) . \tag{30}$$

Figure 7a shows variation along the x-direction of mass fluxes per unit depth obtained from the flow fields computed with 4 techniques. It is obvious that the conventional technique gives the greatest numerical loss of mass flux while the 3 proposed techniques give much smaller variations. There is,

indeed, variation in the mass flux of the proposed techniques as represented in a magnified form in **Figure 8a**.

In accordance with **Figures 7a** and **8a**, it may be concluded that the law of mass conservation is well maintained in the order the 2nd, 3rd and 1st proposed, and conventional techniques, respectively. This is because the conventional technique computes the height function at each position without considering adjacent height functions, leading to a greater numerical loss or gain. While in the 1st proposed method, which requires interpolation for both u and Δz as shown in Eq. (4), there is greater variation of mass flux compared to the other proposed techniques which does not need any interpolation as shown in Eqs. (6) and (8). Finally, the 2nd proposed technique gives a better result than the 3rd proposed technique since the basis of the 2nd proposed technique is second-order accurate.

Considering **Figure 6a** together with **Figure 7a**, it may be concluded that the oscillation of the free surface computed with the proposed techniques next to the inflow boundary is caused by the mass conservation. This oscillation may be diminished by increasing the fineness of the grid resolution. **Figure 6b** shows the surface curves obtained from 4 numerical techniques with a finer grid (30×40 resolution) compared to the exact solution. Now all techniques give a reasonably acceptable free surface curve. This may imply that the grid with 30×40 resolution is fine enough for predicting the flow even if it is uniform.

The variation along the x-direction of mass fluxes per unit depth obtained from the flow fields computed with 4 techniques in the case of the finer grid is shown in **Figure 7b**. It is clear that the result of the conventional technique is greatly improved when the grid is finer. The finer grid also reduces the variation of mass flux obtained from the 1st proposed technique. This is apparent if **Figure 8b** is compared to **Figure 8a**. The finer grid adversely affects the mass flux obtained from the 2nd and 3rd proposed techniques but not to a significant degree.

To get more insight into the influence of the grid resolutions, the relative percent difference;

$$\%\text{Rel.Diff.} = \frac{\left(Max. - Min.\right)}{Avg.} \times 100\%, \tag{31}$$

is employed. **Table 1** shows the comparison of relative percent differences of mass flux computed with 4 numerical techniques between 2 different grids. The influence of grid resolution is very strong in the case of conventional and 1st proposed techniques, the %Ref.Diff. respectively reduces to ~1/5 and ~1/10 times when the grid is finer. While the %Ref.Diff. in the case of the 2nd and 3rd proposed techniques increases only ~2 times when the grid is finer. In addition, the average mass fluxes obtained from the proposed techniques are equal to the exact solution obtained from Eq. (29) for both coarse and fine grids whereas those obtained from the conventional technique are significantly different. This means that the conventional technique requires a much finer grid than the proposed techniques in order to achieve similar accuracy for both surface curve and mass conservation.

Table 1 Comparison of relative percent differences of mass flux computed with 4 numerical techniques using a coarse grid (30×10 resolution) and fine grid (30×40 resolution).

Grid	Technique	Max. (kg/m·s)	Min. (kg/m·s)	Avg. (kg/m·s)	Diff. (kg/m·s)	%Ref.Diff.
30×10	Conventional	6.37×10^{-2}	6.11×10^{-2}	6.15×10^{-2}	2.63×10^{-3}	4.27×10^{0}
	Proposed#1	6.38×10^{-2}	6.37×10^{-2}	6.37×10^{-2}	1.65×10^{-5}	2.59×10^{-2}
	Proposed#2	6.37×10^{-2}	6.37×10^{-2}	6.37×10^{-2}	4.10×10^{-7}	6.43×10^{-4}
	Proposed#3	6.37×10^{-2}	6.37×10^{-2}	6.37×10^{-2}	1.60×10^{-6}	2.51×10^{-3}
30×40	Conventional	6.37×10^{-2}	6.31×10^{-2}	6.32×10^{-2}	5.93×10^{-4}	9.38×10^{-1}
	Proposed#1	6.37×10^{-2}	6.37×10^{-2}	6.37×10^{-2}	1.46×10^{-6}	2.29×10^{-3}
	Proposed#2	6.37×10^{-2}	6.37×10^{-2}	6.37×10^{-2}	1.09×10^{-6}	1.71×10^{-3}
	Proposed#3	6.37×10^{-2}	6.37×10^{-2}	6.37×10^{-2}	3.44×10^{-6}	5.40×10^{-3}

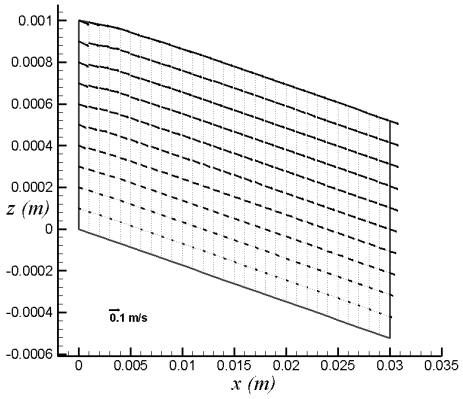

(a) Conventional technique

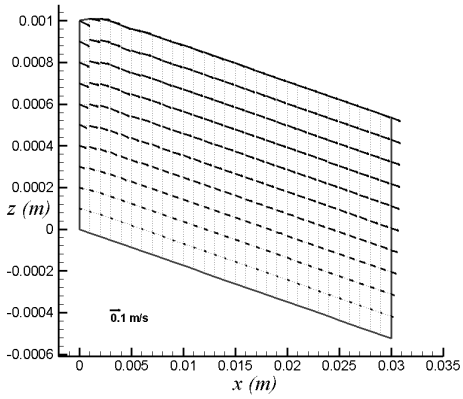

(b) 1st proposed technique

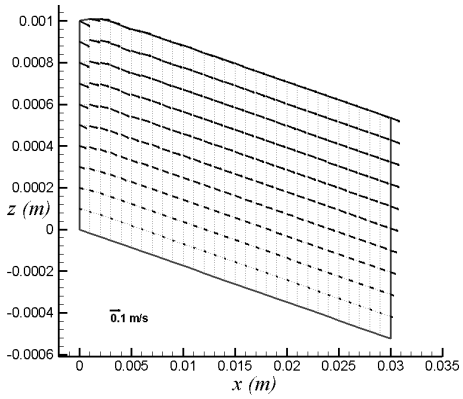

(c) 2nd proposed technique

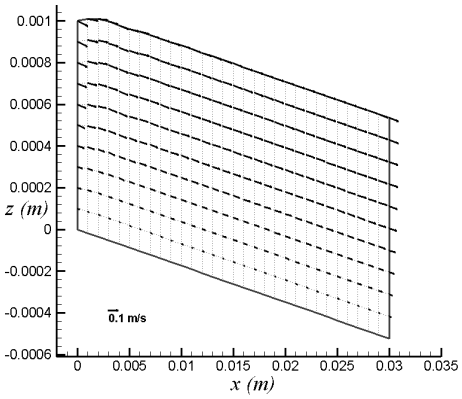

(d) 3rd proposed technique

Figure 5 Velocity field of a thin film flow over an incline in the coarse grid (30×10 resolution) obtained from the height function computed with (a) the conventional technique, (b) the 1st proposed technique, (c) the 2nd proposed technique and (d) the 3rd proposed technique.

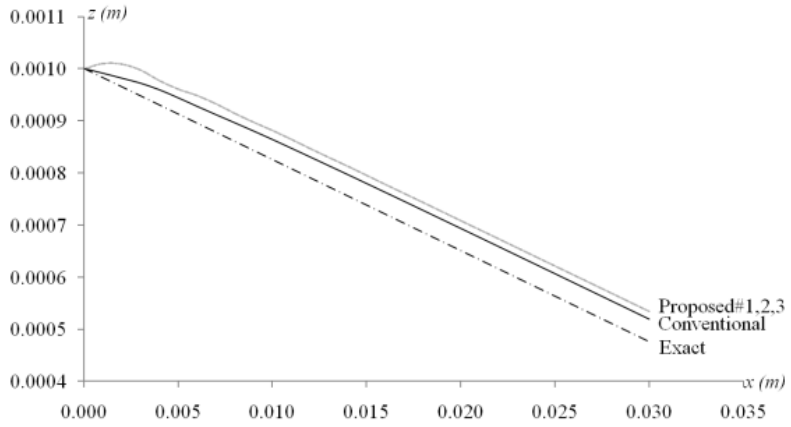

(a) Results for the coarse grid (30×10 resolution)

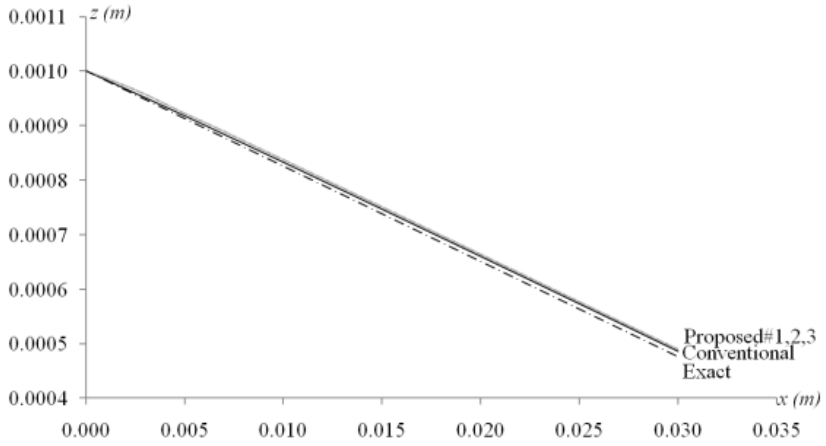

(b) Results for the fine grid (30×40 resolution)

Figure 6 Comparison of free surface curves obtained from 4 numerical techniques and the exact solution for a thin film flow over an incline with (a) the coarse grid and (b) the fine grid.

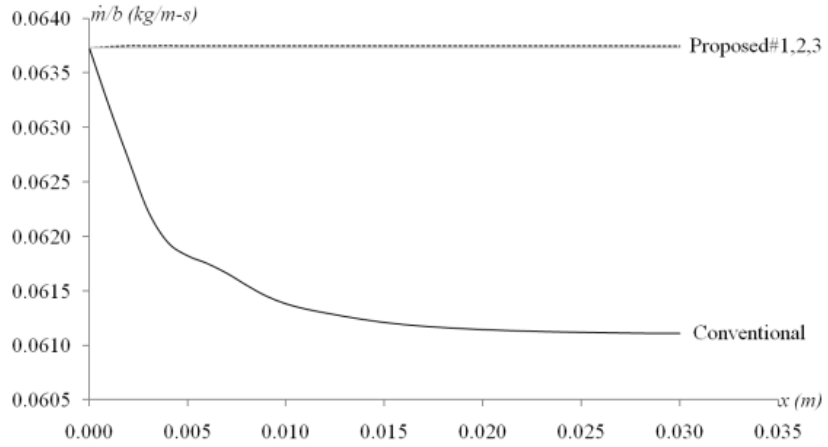

(a) Results for the coarse grid (30×10 resolution)

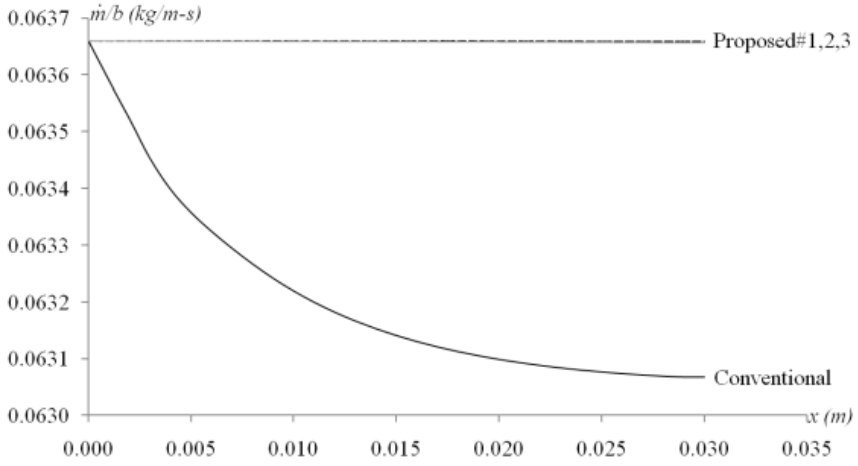

(b) Results for the fine grid (30×40 resolution)

Figure 7 Variation along the x-direction of mass fluxes per unit depth obtained from the flow fields computed with 4 numerical techniques for a thin film flow over an incline with (a) the coarse grid and (b) the fine grid.

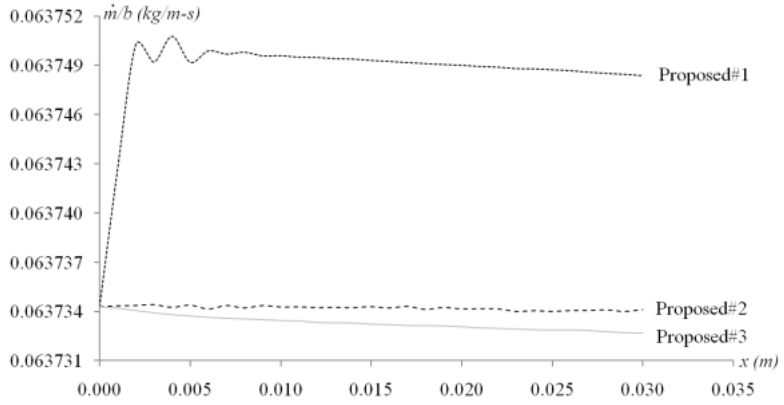

(a) Results for the coarse grid (30×10 resolution)

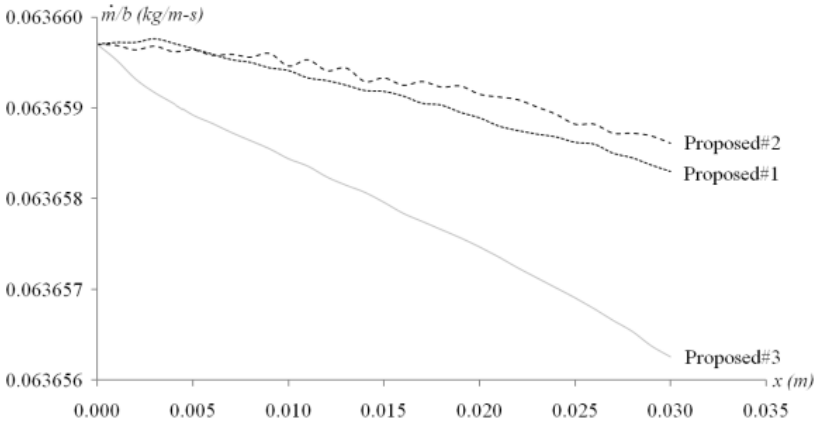

(b) Results for the fine grid (30×40 resolution)

Figure 8 Variation along x-direction of mass fluxes per unit depth obtained from the flow fields computed with 3 proposed techniques for a thin film flow over an incline with (a) the coarse grid and (b) the fine grid.

Examination with complicated problem

After being verified with a simple problem, the numerical techniques are examined with a more complicated problem in this section to prove whether or not the techniques are workable with problems whose exact solution is unknown. A thin film flow over an incline with a weir as shown in **Figure 9** is chosen. Herein, the liquid in the flow is water whose density and viscosity are 997.13 kg/m^3 and 0.891×10^{-3} kg/m·s, respectively. The surface tension on the free surface is 72.14×10^{-3} N/m. The values of the variables in the figure are assigned as $g = 9.81$ m/s^2, $p_{atm} = 0$ Pa, $L_{film} = 1$ cm, $H_{film} = 1$ mm and $\theta =$ 1°. The entrance length, equal to $4\,L_{film}$, is selected because it is expected that the inflow boundary cannot affect the flow field over the weir according to the information obtained from **Figure 6b**.

As illustrated in **Figure 10**, the weir is a circular arc whose curve can be calculated with;

$$z = z_{center} + \sqrt{R_{weir}^2 - \left(x - x_{center}\right)^2}\,, \tag{32}$$

where

$$R_{weir} = \frac{H_{weir}}{2} + \frac{C_{weir}^2}{8H_{weir}},$$
$$C_{weir} = L_{film} \big/ \cos\theta\,,$$
$$x_{center} = x_{weir} - \left(R_{weir} - H_{weir}\right)\sin\theta\,,$$
$$z_{center} = z_{weir} - \left(R_{weir} - H_{weir}\right)\cos\theta\,,$$
$$x_{weir} = \left(9/2\right)L_{film}\,,$$
$$z_{weir} = -\left(9/2\right)L_{film}\tan\theta\,.$$

The grid resolution is 70×40 since this resolution is as fine as the fine grid used in the verification so it is anticipated that the resolution is fine enough even if it is uniform. Boundary conditions are similar to those of the verification. Since an exact solution is not available, initial conditions have to be guessed. Therefore they are set to be similar to the method used in the verification. Each simulated velocity field obtained from 4 numerical techniques is shown in **Figures 11a** to **11d**. The free surface curve violently flutters above the weir in the case of the conventional techniques shown in **Figure 11a**. While the free surface curves above the weir are less wavy in the case of the 3 proposed techniques. However, there is a small-amplitude oscillation of the free surface curve in the upstream region of the flow computed with the 1st proposed technique as shown in **Figure 11b**. This is more obvious in **Figure 12** which is a comparison of free surface curves computed with the 4 numerical techniques. So far, it may be concluded that the wave of the free surface curve will be more violent if only one height function is computed without considering its adjacent height functions. This may be because the adjacent height functions try to restrain the movement of the height function which is being computed. Thus, the interpolation of both u and Δz in the 1st proposed technique causes a small-amplitude oscillation in the upstream region of the weir.

A comparison of the mass fluxes shown in **Figure 13** shows that the conventional technique gives a moderate loss of mass flux in the entrance region at first, and then gives a large loss and a large gain in the region above the weir, before finally giving a moderate loss in the downstream region. The mass fluxes obtained from velocity fields computed with the proposed techniques are apparently more constant. However, the small oscillation in the mass flux of the 1st proposed technique is noticeable. This oscillation is clearer as illustrated in **Figure 14** which is a comparison of mass fluxes from the proposed techniques only. The figure reveals that the 1st proposed technique not only gives oscillation in its result but also its average mass flux is different from the others. The cause of these differences is the interpolation of both u and Δz in the 1st proposed technique as previously mentioned. Nevertheless, the average mass flux of the 1st proposed technique is just 0.1 % different from those of the other proposed techniques, so the difference is not significant.

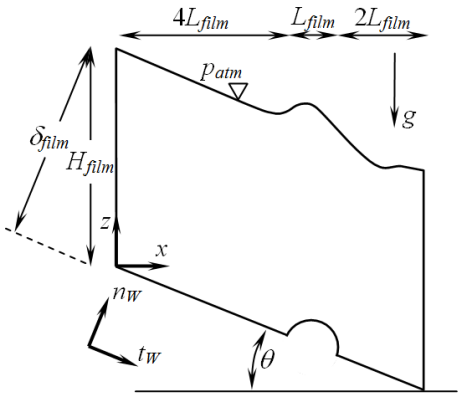

Figure 9 Computational domain of a thin film flow over an incline with a weir.

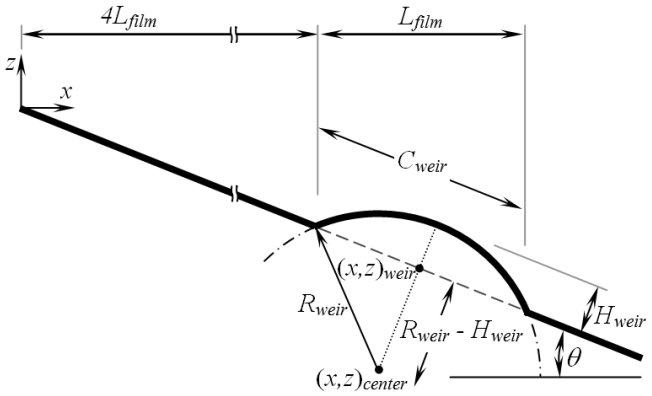

Figure 10 Dimension of the circular weir on the incline.

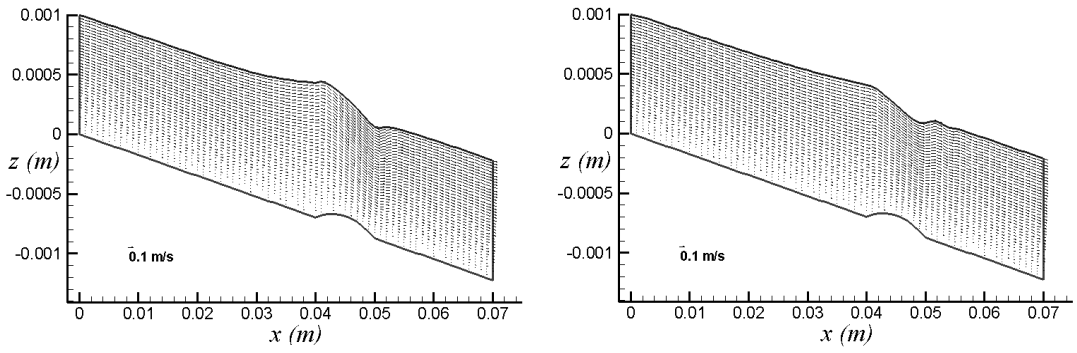

(a) Conventional technique

(c) 2nd proposed technique

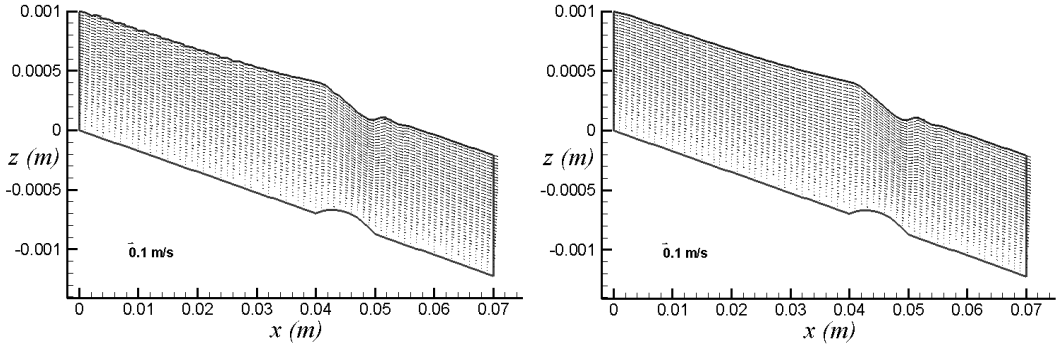

(b) 1st proposed technique (d) 3rd proposed technique

Figure 11 Velocity field of a thin film flow over an incline with a weir obtained from height function computed with (a) the conventional technique, (b) the 1st proposed technique, (c) the 2nd proposed technique and (d) the 3rd proposed technique.

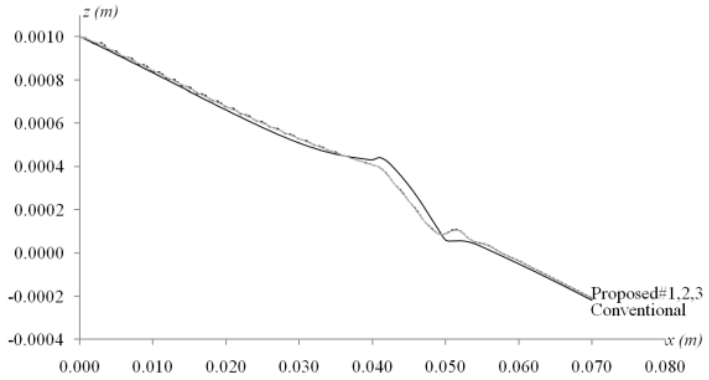

Figure 12 Comparison of free surface curves obtained from the 4 numerical techniques for a thin film flow over an incline with a weir.

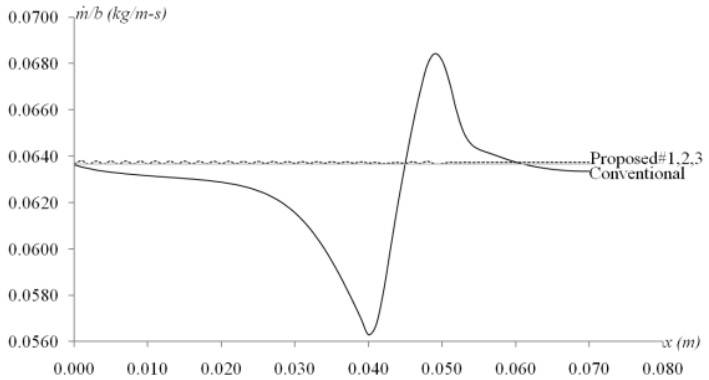

Figure 13 Variation along the x-direction of the mass fluxes per unit depth obtained from the flow fields computed with the 4 numerical techniques for a thin film flow over an incline with a weir.

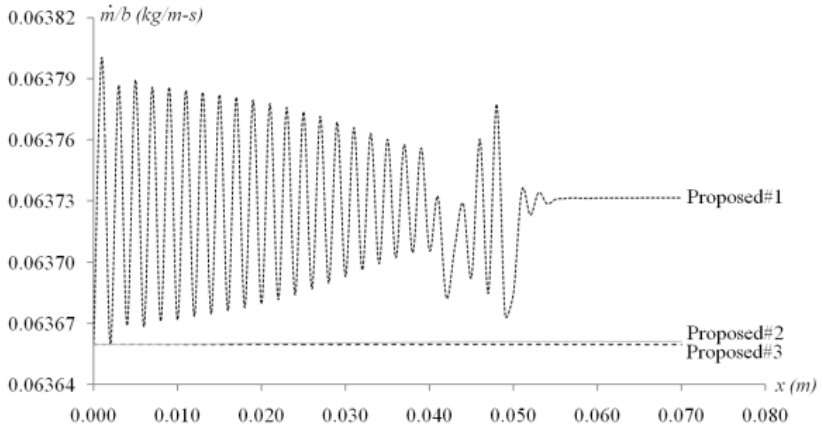

Figure 14 Variation along the x-direction of mass fluxes per unit depth obtained from the flow fields computed with the 3 proposed techniques for a thin film flow over an incline with a weir.

Conclusions

Three proposed techniques were developed for maintaining the law of mass conservation. By comparing them to one another as well as to the conventional technique, it is found that:

1. The proposed techniques give better results than the conventional technique does since:

1.1. The mass fluxes per unit depth obtained from the velocity field computed with the proposed techniques are well conserved. Whereas, those of the conventional technique are not constant even in the case where the free surface curve is still a straight line.

1.2. The shapes of the free surface curve obtained from the proposed techniques are less wavy than those obtained from the conventional technique. This may be due to the restraint of adjacent height functions which are neglected in the conventional technique.

However, caution is required in applying the proposed techniques as they require a sufficiently fine grid in the vertical direction. Using too coarse grids with the proposed techniques may cause fluttering of the free surface in the region close to the inflow boundary since the proposed techniques try to conserve mass flux. This is proved by comparing the simulation results in the coarse grid (30×10 resolution) and those in the finer grid (30×40 resolution).

2. Among the proposed techniques, the 1st proposed technique gives the worst result due to the linear interpolation of both u and Δz. The weakness is more apparent in the case where nonlinearity dominates. It is expected that the 1st proposed technique could be improved by applying an interpolation scheme with a higher-order accuracy. However, this requires more effort.

3. Although both the 2nd and 3rd proposed techniques give acceptable results, the 2nd proposed technique gives comparatively better results due to the second-order nature of the accuracy scheme. The 3rd proposed technique is, however, easier to use due to its explicit form.

Recently, the height function method, which is a surface tracking method, is not only used alone but also blended with surface capturing methods. The VOF method, which is a surface capturing method, is often blended with the height function. The combination of both techniques leads to utilizing their strong points, i.e. the VOF method possesses superior mass conservation properties while the height function is good at estimating surface curvatures [18]. The combination needs algorithms for transmitting information from the VOF method to the height function and vice versa. One of basic algorithms used is the continuum surface force (CSF) with a piecewise linear interface calculation (PLIC) [24]. The algorithm is simple but brings a formidable problem that is discontinuity of surface curves, resulting in unrealistic surface shapes. To solve the problem, several algorithms have been developed and proposed. For example, the height function is shifted to lie outside grid cells but this needs more complicated

techniques which are still being developed at present [18]. Another way to solve the problem of unrealistic surface shapes is using an adaptive grid [20] but this consumes computational resources in return.

References

[1] R Scardovelli and S Zaleski. Direct numerical simulation of free-surface and interfacial flow. *Annu. Rev. Fluid Mech.* 1999; **31**, 567-603.
[2] H Lan and Z Zhang. Comparative study of the free-surface boundary condition in two-dimensional finite-difference elastic wave field simulation. *J. Geophys. Eng*. 2011; **8**, 275-86.
[3] FH Harlow and JE Welch. Numerical calculation of time-dependent viscous incompressible flow of fluid with free surface. *Phys. Fluid*. 1965; **8**, 2182-9.
[4] J Lin, Y Kamotani and S Ostrach. An experimental study of free surface deformation in oscillatory thermocapillary flow. *Acta Astronaut*. 1995; **35**, 525-36.
[5] T Hazuku, T Takamasa and K Okamoto. Simultaneous measuring system for free surface and liquid velocity distributions using PIV and LFD. *Exp. Therm. Fluid. Sci*. 2003; **27**, 677-87.
[6] JM Campin, A Adcroft, C Hill and J Marshall. Conservation of properties in a free-surface model. *Ocean. Model*. 2004; **6**, 221-44.
[7] S Smolentsev and R Miraghaie. Study of a free surface in open-channel water flows in the regime from "Weak" to "Strong" turbulence. *Int. J. Multiphas. Flow* 2005; **31**, 921-39.
[8] L Lu, Y Li and B Teng. Numerical simulation of turbulent free surface flow over obstruction. *J. Hydrodyn*. 2008; **20**, 414-23.
[9] F Murzyn and H Chanson. Free-surface fluctuations in hydraulic jumps: Experimental observations. *Exp. Therm. Fluid. Sci*. 2009; **33**, 1055-64.
[10] SH Sadathosseini, SM Mousaviraad, B Firoozabadi and G Ahmadi. Numerical simulation of free-surface waves and wave induced separation. *Sci. Iran*. 2008; **15**, 323-31.
[11] S Mayer, A Garapon and LS Sorensen. A fractional step method for unsteady free-surface flow with applications to non-linear wave dynamics. *Int. J. Numer. Meth. Fluid.* 1998; **28**, 293-315.
[12] E Aulisa, S Manservisi and R Scardovelli. A surface marker algorithm coupled to an area-preserving marker redistribution method for three-dimensional interface tracking. *J. Comput. Phys*. 2004; **197**, 555-84.
[13] PE Raad, S Chen and DB Johnson. The introduction of the micro cells to treat pressure in free surface fluid flow problems. *J. Fluid. Eng*. 1995; **117**, 683-90.
[14] BD Nichols and CW Hirt. Calculating three-dimensional free surface flows in the vicinity of submerged and exposed structures. *J. Comput. Phys*. 1971; **12**, 234-46.
[15] S McKee, MF Tome, VG Ferreira, JA Cuminato, A Castelo, FS Sousa and N Mangiavacchi. The MAC method. *Comput. Fluid*. 2008; **37**, 907-30.
[16] CW Hirt and BD Nichols. Volume of fluid (VOF) method for the dynamics of free boundaries. *J. Comput. Phys*. 1981; **39**, 201-25.
[17] P Liovic, M Rudman and JL Liow. Numerical modelling of free surface flows in metallurgical vessels. *In:* Proceedings of the 2nd International Conference on CFD in the Minerals and Process Industries CSIRO, Melbourne, Australia, 1999, p. 255-60.
[18] SJ Cummins, MM Francois and DB Kothe. Estimating curvature from volume fractions. *Comput. Struct.* 2005; **83**, 425-34.
[19] S Afkhami and M Bussmann. Height function-based contact angles for VOF simulations of contact line phenomena. *In:* Proceedings of the 5th International Conference on Scientific Computing and Applications, Banff Alberta, Canada, 2006.
[20] S Afkhami and M Bussmann. Height functions for applying contact angles to 2D VOF simulations. *Int. J. Numer. Meth. Fluid.* 2008; **57**, 453-72.
[21] PA Ferdowsi and M Bussmann. Second-order accurate normals from height functions. *J. Comput. Phys*. 2008; **227**, 9293-302.

[22] J López, C Zanzi, P Gómez, R Zamora, F Faura and J Hernández. An improved height function technique for computing interface curvature from volume fractions. *Comput. Meth. Appl. Mech. Eng*. 2009; **198**, 2555-64.
[23] JH Ferziger and M Perić. *Computational Methods for Fluid Dynamics*. 3rd ed. Springer-Verlag Berlin Heidelberg New York, Germany, 2002, p. 381-2.
[24] S Afkhami and M Bussmann. Height Functions for applying contact angles to 3D VOF simulations. *Int. J. Numer. Meth. Fluid.* 2009; **61**, 827-47.